Alkanethiolate Reorientation during Metal Electrodeposition

ARTICLE *in* LANGMUIR · JANUARY 2002

Impact Factor: 4.46 · DOI: 10.1021/la0109819

6 AUTHORS, INCLUDING:

Alexander M Bittner
CIC nanoGUNE Consolider
74 PUBLICATIONS **3,298** CITATIONS
SEE PROFILE

A. Tadjeddine
Université Paris-Sud 11 and CNRS
174 PUBLICATIONS **3,148** CITATIONS
SEE PROFILE

Alkanethiolate Reorientation during Metal Electrodeposition

Maximilian Epple,[†] Alexander M. Bittner,*[,†,‡] Klaus Kuhnke,[†,‡] Klaus Kern,[†,‡] Wan-Quan Zheng,[§,||] and Abderrahmane Tadjeddine[§]

Institut de Physique Expérimentale, Ecole Polytechnique Fédérale de Lausanne (EPFL), CH-1015 Lausanne, Switzerland, Laboratoire pour l'Utilisation du Rayonnement Electromagnétique (LURE), CLIO, F-91898 Orsay CEDEX, France, and Laboratoire de Photophysique moléculaire, Université Paris Sud, Bât. 210+350, F-91405 Orsay CEDEX, France

Received June 27, 2001. In Final Form: November 9, 2001

By use of spectroscopic sum frequency generation, we studied the molecular orientation in alkanethiolate self-assembled monolayers (SAMs) on Au(111) in situ during copper electrodepositon. The study is combined with an in situ scanning tunneling microscopy investigation under similar experimental conditions providing complementary real-space information. For the shortest molecule, hexanethiol (C6), an increase of the methyl group tilt angle during copper deposition from 22° to 83° is observed. Control experiments exclude a purely potential-induced origin indicating that Cu adsorption triggers the reorientation. The result is compatible with a rotation of the alkyl chain around its long axis accompanied by a change of surface−S−C angle. The structural change is partially reversible by copper stripping. The study demonstrates that slow metal deposition in the submonolayer range can have a major impact on the adsorbate structure of short chain thiolates.

1. Introduction

Self-assembled monolayers (SAMs) of molecules are investigated for purposes as different as sensors,[1] corrosion protection,[2,3] nanostructuring,[4−8] catalysis,[9,10] or membrane modeling. Possible electrochemical applications in batteries or capacitors or for galvanic deposition but also for corrosion protection and surface biochemistry call for a better understanding of the surface−adsorbate−electrolyte system.

It has been established that adsorbed layers can become reversibly modified by contact to solvents.[11−13] The application of monolayers in electrochemistry, however, submits the layer to probably even stronger constraints due to electrochemical potential and processes accompanying metal deposition. Not much is known yet about these processes and the role the adsorbed layer plays in it. The occurrence of metal deposition might require or be accompanied by a specific response of the adlayer, e.g., adsorbate displacement, other structural and conformational adjustments, or even desorption. This study tries to shed some light onto these processes by investigating the conformation and orientation of alkanethiolate molecules within SAMs before and especially during the electrochemical deposition of a metal. We chose copper deposition onto alkanethiolate SAMs adsorbed on Au(111) as a model system for metal electrodepositon.[14−16] Alkanethiolate SAMs combine simple preparation with a relatively high chemical and physical stability. The widely employed standard copper deposition in sulfuric acid solution allows a comparison of our results with earlier studies. The system is thus well defined with respect to substrate (single crystal), organic layer (monomolecular), and deposited metal (well-characterized coverage−structure relation, e.g., submonolayer islands). The high sensitivity to geometrical changes of molecular groups and the fact that the study must be undertaken with the surface exposed to the electrolyte makes infrared sum frequency generation (SFG) spectroscopy the method of choice. Since isotropically arranged molecules (e.g., in a liquid phase) give no SFG signal, the method is selective to molecules adsorbed at an interface. Finally, this study includes STM results to prove the actual deposition of Cu on the substrate under the employed experimental conditions.

A "C*n* thiol" $CH_3(CH_2)_{n-1}SH$ adsorbs from solution or from the gas phase as thiolate $CH_3(CH_2)_{n-1}S$/Au(111),

* To whom correspondence may be addressed. E-mail: a.bittner@fkf.mpg.de.

[†] Ecole Polytechnique Fédérale de Lausanne.

[‡] Present address: Max Planck-Institut für Festkörperforschung, Heisenbergstr. 1, D-70569 Stuttgart, Germany.

[§] Laboratoire pour l'Utilisation du Rayonnement Electromagnétique.

[||] Université Paris Sud.

(1) Wink, T.; v. Zuilen, S. J.; Bult, A.; v. Bennekom; W. P. *Analyst* **1997**, *122*, 34R.

(2) Scherer, J.; Vogt, M. R.; Magnussen, O. M.; Behm, R. J. *Langmuir* **1997**, *13*, 7045.

(3) Jennings, G. K.; Munro, J. C.; Yong, T.-H.; Laibinis, P. E. *Langmuir* **1998**, *14*, 6130.

(4) Piner, R. D.; Zhu, J.; Xu, F.; Hong, S.; Mirkin, C. A. *Science* **1999**, *283*, 661.

(5) Maoz, R.; Cohen, S. R.; Sagiv, J. *Adv. Mater.* **1999**, *11*, 55.

(6) Eberhardt, A. S.; Nyquist, R. M.; Parikh, A. N.; Zawodzinski, T.; Swanson, B. I. *Langmuir* **1999**, *15*, 1595.

(7) Biebuyck, H. A.; Larsen, N. B.; Delamarche, E.; Michel, B. *IBM J. Res., Dev.* **1997**, *41*, 159.

(8) Kumar, A.; Biebuyck, H. A.; Whitesides, G. M. *Langmuir* **1994**, *10*, 1498.

(9) Dressick, W. J.; Dulcey, C. S.; Georger, J. H.; Calabrese, G. S.; Calvert, J. M. *J. Electrochem. Soc.* **1994**, *141*, 210. Hidberg, P. C.; Helbig, W.; Kim, E.; Whitesides, G. M. *Langmuir* **1996**, *12*, 1375.

(10) Kind, H.; Bittner, A. M.; Cavalleri, O.; Kern, K.; Greber, T. *J. Phys. Chem. B* **1998**, *102*, 7582.

(11) Hines, M. A.; Todd, J. A.; Guyot-Sionnest, P. *Langmuir* **1995**, *11*, 493.

(12) Anderson, M. R.; Gatin, M. *Langmuir* **1994**, *10*, 1638.

(13) Anderson, M. R.; Evaniak, M. N.; Zhang, M. *Langmuir* **1996**, *12*, 2327.

(14) Cavalleri, O.; Gilbert, S. E.; Kern, K. *Chem. Phys. Lett.* **1997**, *269*, 479.

(15) Cavalleri, O.; Kind, H.; Bittner, A. M.; Kern, K. *Langmuir* **1998**, *14*, 7292.

(16) Cavalleri, O.; Bittner, A. M.; Kind, H.; Kern, K.; Greber, T. *Z. Phys. Chem.* **1999**, *208*, 107.

10.1021/la0109819 CCC: $22.00
Published on Web 01/10/2002

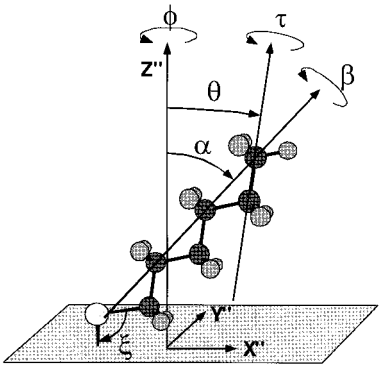

Figure 1. Angles defining the molecular and the methyl group orientation for a thiolate at a surface. Three angles define the orientation of the molecule in all-trans conformation: tilt or cant (α), the twist (β), and the azimuth (ϕ). The methyl group orientation is defined by tilt (θ), twist (τ), and azimuth (ϕ). The coordinates x'', y'', z'' represent the surface coordinate system.

referred to as a "C*n* SAM", creating a strong S−Au bond and lifting the Au(111) reconstruction. The sulfur atom is usually thought to be located in 3-fold hollow sites Au_3.[17−19] However, this has recently been questioned.[20−22] For our purposes, we do not need exact information on the adsorption site but it is important to keep in mind the adsorption strength and a non-negligible mobility of the sulfur moiety on the gold surface. This mobility is responsible for the formation of a well-ordered SAM and thus also for the formation of sulfur arrangements that differ from the usual $(\sqrt{3} \times \sqrt{3})$R30° lattice, such as the so-called striped structures, mainly observed for small *n* or low coverages.[23]

The surface−S−C angle is believed to be close to the tetrahedral angle 110°. Theoretical studies, however, suggest the possibility of the presence of both 110° and 180° angles.[19,24] The molecular backbone C*n* is in the all-trans conformation, hence a C−C−C plane can be defined, and the molecule may be visualized as a rod. The orientation of the molecule (Figure 1) is described by three angles: The tilt or cant α between the molecular axis (or rod) and the surface normal, the azimuth ϕ (angle with respect to a given surface crystallographic orientation), and the twist β of the C−C−C plane around the rod's axis. Generalizing the experimental findings for adsorption from thiol solutions, we can say that in the long-chain regime ($n > 14$) sulfur arranges mostly in a $(\sqrt{3} \times \sqrt{3})$-R30° lattice,[23,25−30] often arranged in a c(4 × 2) superstructure. This results in a coverage of 1/3 with respect to the Au(111)−(1 × 1) lattice to which we refer throughout this work. The S−S distance is too large to allow a stable packing of vertical methylene chains on gold, hence the tilt α is ≈30°,[25,29,31−33] which results in a maximized van der Waals interaction between the methylene chains. The chain−chain distance is now close to the alkane bulk value,[29,34] and the structure is reminiscent of that of bulk alkanes.[34,35] The tilt α is directed toward the S−S next-nearest neighbor, i.e., in the [1$\bar{1}$0] direction of the densely packed gold rows; this direction (angle ϕ) varies slightly with *n*.[29] The twist angle β determined from infrared spectra is ≈50°.[25,31−33] Experimental[32] and theoretical evidence[24,36] as well as the alkane bulk structure suggest an alternative model where a chain and its neighbor exhibit angles of +45° and −45°, respectively.

For alkanethiols the contact with solvents or electrolytes does not cause drastic changes of the structure; in fact, aqueous solutions result in a barely measurable broadening of some spectral features while STM images show no changes. More important are changes brought about by the electrochemical potential; Hines et al.[11] showed that SFG spectra in diluted $HClO_4$ remain unchanged only from −200 to 1100 $mV_{Cu/Cu^{2+}}$.[37] Below −200 mV thiolate layers become damaged, and they can desorb reductively at very negative potentials in basic electrolytes,[38] while above 1100 mV they are oxidatively damaged.[39] Such changes are irreversible and correspond to "strong activation" according to Cavalleri et al.[16] In contrast, we present here orientational changes at potentials where electrodeposition can be finely tuned and potential induced damage does not yet occur.

2. Experimental Section

2.1. Sample Preparation. Gold single crystals were cleaned in oxidizing acidic solution (Nochromix (Thomas Scientific) in concentrated H_2SO_4) and flame annealed. For the self-assembly, the gold samples (and a gold wire that connects the sample electrically) were transferred into 10 μM up to 1 mM ethanolic solutions of alkanethiols (Fluka), $CH_3(CH_2)_{n-1}SH$, with $n = 6$, 12, and 18. The temperature was held at ≈320 K for 1 or 2 days, thereafter at 300 K for some hours up to several weeks. Directly before an experiment, a sample was emersed, rinsed with ethanol, and mounted. It was brought in contact with the electrolyte, 50 mM H_2SO_4 (p.a., Fluka) + 0 or 1 mM $CuSO_4$ (p.a., Fluka) in water (Millipore). In the copper-containing solution the reference electrode was a copper wire, etched in HNO_3 and rinsed with water shortly before use. In the copper-free solution the reference was a Pd wire at which hydrogen had been evolved for at least 30 min.[40] For consistency we quote all potentials against the Cu/Cu^{2+} (1 mM) potential (0 mV reads +250 mV on the standard hydrogen scale). We employed an EG&G PAR 400 potentiostat. When not mentioned explicitly, +400 mV was applied for at least 1 h before SFG or STM experiments were started.

The electrochemical cell for the optical setup (Figure 2) is made of poly(chlorotrifluoroethylene) (PCTFE) with a platinum or gold counter electrode. While during electrochemical preparation the

(17) Bhatia, R.; Garrison, B. J. *Langmuir* **1997**, *13*, 4038.
(18) Bhatia, R.; Garrison, B. J. *Langmuir* **1997**, *13*, 765.
(19) Sellers, H.; Ulman, A.; Shnidman, Y.; Eilers, J. E. *J. Am. Chem. Soc.* **1993**, *115*, 9389.
(20) Yeganeh, M. S.; Dougal, S. M.; Polizzotti, R. S.; Rabinowitz, P. *Phys. Rev. Lett.* **1995**, *74*, 1811.
(21) Kluth, G. J.; Carrano, C.; Marboudian, R. *Phys. Rev. B* **1999**, *59*, R10449.
(22) Fenter, P.; Schreiber, F.; Berman, L.; Scoles, G.; Eisenberger, P.; Bedzyk, M. *Surf. Sci.* **1998**, *412/413*, 213.
(23) Schreiber, F. *Prog. Surf. Sci.* **2000**, *65*, 151.
(24) Li, T.-W.; Chao, I.; Tao, Y.-T. *J. Phys. Chem. B* **1998**, *102*, 2935.
(25) Dubois, L. H.; Nuzzo, R. G. *Annu. Rev. Phys. Chem.* **1992**, *43*, 437.
(26) Cavalleri, O.; Hirstein, A.; Bucher, J.-P.; Kern, K. *Thin Solid Films* **1996**, *284/285*, 392.
(27) Camillone, N.; Eisenberger, P.; Leung, T. Y. B.; Schwartz, P.; Scoles, G.; Poirier, G. E.; Tarlov, M. J. *J. Chem. Phys.* **1994**, *101*, 11031.
(28) Gerlach, R.; Polanski, G.; Rubahn, H.-G. *Appl. Phys. A* **1997**, *65*, 375.
(29) Fenter, P.; Eberhardt, A.; Liang, K. S.; Eisenberger, P. *J. Chem. Phys.* **1997**, *106*, 1600.
(30) Poirier, G. E. *Chem. Rev.* **1997**, *97*, 1117.
(31) Laibinis, P. E.; Whitesides, G. M.; Allara, D. L.; Tao, Y.-T.; Parikh, A. N.; Nuzzo, R. G. *J. Am. Chem. Soc.* **1991**, *113*, 7152.
(32) Terrill, R. H.; Tanzer, T. A.; Bohn, P. W. *Langmuir* **1998**, *14*, 845.
(33) Thome, J.; Himmelhaus, M.; Zharnikov, M.; Grunze, M. *Langmuir* **1998**, *14*, 7435.
(34) Ewen, B.; Strobl, G. R.; Richter, D. *Faraday Discuss. Chem. Soc.* **1980**, *69*, 19.
(35) Snyder, R. G. *J. Chem. Phys.* **1979**, *71*, 3229.
(36) Mar, W.; Klein, M. L. *Langmuir* **1994**, *10*, 188.
(37) For better comparison, we quote all potentials with respect to a hypothetical Cu/Cu^{2+} (1 mM) reference (=0 mV_{Cu}, =250 mV vs SHE).
(38) Walczak, M. M.; Chung, C.; Stole, S. M.; Widrig, C. A.; Porter, M. D. *J. Am. Chem. Soc.* **1991**, *113*, 2370.
(39) Gilbert, S. E.; Cavalleri, O.; Kern, K. *J. Phys. Chem.* **1996**, *100*, 12123.
(40) Testing the obtained Pd/H electrode showed an offset of ±100 mV and in some experiments also a drift of ca. −40 mV/h. For this we corrected the potentials given in this paper.

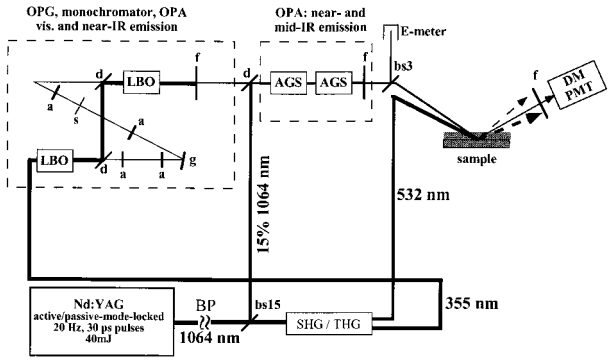

Figure 2. Schematic drawing of the experimental setup: BP, improvement of beam quality (see text); bs15, beam splitter 15%; SHG/THG, frequency doubling and tripling with KD*P crystals; LBO, LiB_3O_5 crystal; d, dielectric mirror; a, achromatic lens; g, grating 1200 lines/mm; s, slit 50 μm width; f, filter blocking the pump beam; AGS, $AgGaS_2$ crystal; bs3, beam splitter 3%; E, energy meter monitoring infrared pulse energy; DM, double monochromator; PMT, photomultiplier tube.

surface must be covered by a thick electrolyte layer, for the SFG measurements an equilateral CaF_2 prism is lightly pressed against the horizontally mounted sample surface in order to minimize infrared absorption in the electrolyte. The prism is mounted in a freely rotating gimbal mount (two rotational degrees of freedom). When the prism is lowered onto the sample, the mount allows the prism surface to adjust parallel to the sample surface while avoiding sample scratches that would occur if the prism was able to slide. The amount of electrolyte between surface and prism is determined by the macroscopic roughness of the sample and the prism face.

2.2. Measurements on C6 and C18 SAMs. In the C6 and C18 SAM experiments performed at EPFL, a two-stage optical parametric device similar to that used in refs 41 and 42 was used. As shown in Figure 2, the system is driven by an active passive mode locked Nd:YAG laser (Continuum PY-20) with an amplifier which generates single pulses at a fundamental wavelength of 1.064 μm and a repetition rate of 20 Hz. The duration of the pulses is 35 ps, and the energy is around 40 mJ. The beam is frequency doubled and tripled in potassium dideuterium phosphate (KD*P, KD_2PO_4) crystals. To obtain a spatially smooth intensity distribution in the third harmonic beam, it is necessary to improve the spatial quality of the fundamental beam. This is done by blocking the outer part of the beam with a 4 mm aperture before reducing the beam diameter with a telescope by a factor of 2 and letting the beam propagate for 8 m. The frequency-tripled pulses of 5 mJ energy at 355 nm pump the first stage of the optical parametric device, an optical parametric generation and amplification (OPG/OPA) unit, which consists of two lithium triborate (LBO, LiB_3O_5) crystals. The spectral bandwidth is set to 12 cm^{-1} by a monochromator built between the two LBO crystals. The generated wavelength is tuned from 0.4 to 2.0 μm by rotating the crystals and the monochromator grating.

These pulses seed the second stage, an angle-tuned optical parametric amplifier (OPA) consisting of two silver gallium thiolate ($AgGaS_2$) crystals that are pumped by 3 mJ pulses split off the fundamental of the laser (see Figure 2). From this stage pulses tunable from 1100 to 4600 cm^{-1} (idler component) are obtained. In the range between 2750 and 3100 cm^{-1} the available energy per pulse after a long pass filter is about 100 μJ (spectral width 12 cm^{-1}). Operating the system almost daily during more than 1 year at this energy did not result in any visible crystal degradation such as surface blackening that is often reported for similar systems. However, the reduced output power resulted in prolonged measuring times for SFG spectra.

A part of the doubled fundamental Nd:YAG beam is used as a visible up-conversion pulse ($\lambda = 532$ nm) to generate the SFG signal at the sample. The visible (vis) beam is parallel and p-polarized with an energy density on the sample of about 5 mJ/cm^2 over a beam diameter of about 3 mm. It passes through a 532 nm band-pass "laser line" filter suppressing any background at the sum frequency. It impinges at an angle of 62° with respect to the sample surface onto an equilateral prism pressed with one side onto the sample. The incidence angle on the sample covered with a thin layer of electrolyte (refractive index of water n=1.34) is thus at 70° with respect to the surface normal. The polarization of the infrared beam is linear as defined by the parametric generation process and selected to be p-polarized on the sample. It is slightly focused to a beam diameter of about 1 mm on the surface (typical energy density 10mJ/cm^2). The incidence angle in the electrolyte with respect to the surface normal is 56°. The two beams are incident in the same plane, and for the spectra presented in this paper both are p-polarized. The emitted p-polarized SF signal passes through a 532 nm notch filter and a high pass filter reducing stray light before it passes into a double monochromator. The photomultiplier pulses are measured with a gated charge integrator (Camac, LeCroy ADC 2249 SG). We limited the power density of the incident beams on the surface so that roughly 10 SFG photons per pulse from the gold substrate are measured. Under these conditions no beam-induced degradation of the thiolate layer was observed.

As the shot-to-shot intensity variations are larger for the tunable infrared beam (typically 16% root mean square) than for the visible beam (7% root mean square), a simple but effective noise reduction was achieved by rejecting all pulses from signal averaging in which the infrared energy was below a certain threshold (typically 50% of the average shot energy). In addition the SFG signal for each laser shot was normalized to the intensity of a monitor beam split off (3%) the infrared beam.

In situ SFG spectra of $CH_3(CH_2)_{n-1}S$/Au(111) were taken after the sample had been immersed in electrolyte and held at a defined potential. For potentials above 200 mV (no copper deposition), the minimal holding time was 15 min; for all other potentials the minimal time was 1 h. These times were chosen on the basis of typical copper deposition rates observed by scanning tunneling microscopy (STM).[14,16,39] After this holding time, the CaF_2 prism was lowered onto the surface, reducing the current and the amount of electrolyte available above the surface but keeping potential control. Recording SFG spectra took typically 2 h per potential before the prism was lifted again and the potential was changed. The potentials were chosen similar to those employed in our earlier STM studies.[14−16,39] The spectra are averaged over several separate measurements covering 2−10 h acquisition time.

2.3. Evaluation of the SFG Data. The electrolyte film between the surface and prism due to their macroscopic surface roughness can lead to absorption of the infrared beam. This fact is illustrated by the continuous signal decrease with increasing wavenumbers in the C18 SAM spectrum in Figure 3. The corresponding water absorption line is centered around 3400 cm^{-1}. The spectrum is dominated by the nonresonant SFG signal from the gold substrate surface on which the thiolate resonances appear as inverted peaks. In the measured spectral range the signal from gold is essentially independent of frequency if measured in air. To present spectra in which the thiolate resonances are clearly discernible, the spectra were fitted by the corresponding part of the infrared absorption curve of water and then divided by the fitted curve. It was found that fitting simply with a slowly varying polynomial (usually of order 5) is more efficient and gives a similar result. Except for Figure 3, only these normalized spectra are presented in this paper. We made sure that the procedure preserves the SFG vibrational resonances while the signal attenuation due to the infrared absorption of water is removed. As the fitting procedure provides a mean intensity of the normalized spectrum of 1, strong inverted peaks can create broad positive peaks in their wings. One has to be aware of such artifacts when evaluating the spectra.

2.4. Measurements on C12 SAMs. Experiments were also carried out at LURE-CLIO (Orsay) in order to confirm the results obtained with the OPG/OPA and to study the C_{12} SAM system. Here, an optical parametric oscillator (OPO) was employed. An active passive mode locked Nd:YAG laser delivers a train of pulses to a rotatable lithium niobate ($LiNbO_3$) crystal that is placed in a near-infrared cavity (ca. 4700−6800 cm^{-1}). The corresponding mid-infrared pulses of ca. 4700−2600 cm^{-1}

(41) Krause, H.-J.; Daum, W. *Appl. Phys. Lett.* **1992**, *60*, 2180.
(42) Himmelhaus, M. Ph.D. Thesis, University of Heidelberg (Germany), 1997.

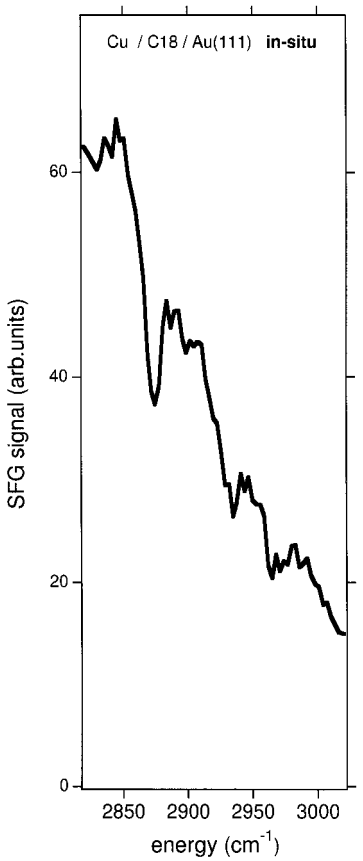

Figure 3. SFG spectrum of C18 SAM/Au(111) in situ in a copper solution at the open circuit potential (+400 mV vs Cu^{2+}/Cu potential). The SFG signal is presented as it is recorded and represents an average over several measurements. The slope of the background is due to absorption in the aqueous solution. After normalization as described in the text the upper spectrum in Figure 4 is obtained.

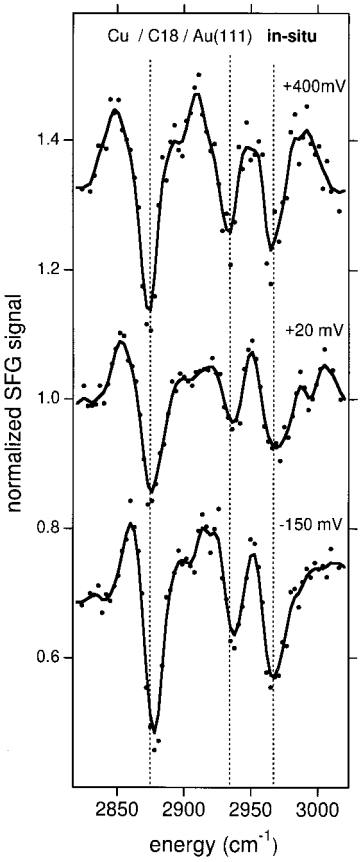

Figure 4. SFG spectra of C18 thiolate SAM/Au(111) in situ in a copper solution at different electrochemical potentials. All data are normalized to the gold substrate signal. The dots are the original data; the lines are smoothed data. The average value of all traces is 1; to represent the spectra in one graph, spectra have been shifted upward or downward for clarity.

have a duration of 11 ps and a width of 2 cm^{-1}. They are mixed on the sample with 10 ps long pulses of the doubled fundamental. Beam geometry and detection are similar to the OPG/OPA setup (EPFL). The SFG signal is normalized to a reference signal generated by mixing a part of the infrared *and* the visible beam in a ZnS plate. The electrochemical cell has a closed design with a vertically oriented sample surface. For more details see ref 43.

2.5. Measurements by STM. Samples were prepared by evaporation of 120−150 nm gold in a vacuum (10^{-5} mbar) on 570 K hot cleaved mica and then annealed for several hours at 600 K (2×10^{-6} mbar). Large (111)-oriented terraces were obtained. In some cases, directly before starting the self-assembly, the gold films were additionally flame annealed at very dark red glow and cooled in air which, however, was found to reduce the defect (step) density only marginally. On finding this, we abandoned this part of the procedure. The self-assembly was carried out as for the SFG studies. STM measurements were performed as described in ref 39. The sample was mounted in a PCTFE cell equipped with a Pt counter electrode and a Pd/H reference. The STM tips were etched and polymer-coated Pt/Ir wires. STM images in this paper are shown as derivative: steps descending from left to right show up as black lines, ascending ones as white lines.

3. Results

3.1. SFG. 3.1.1. Observed Resonances. Figure 4 top shows a C18 SAM spectrum in copper/sulfuric acid solution at a potential at which no copper is deposited (+400 mV). The spectrum exhibits three peaks. Due to the interference[11] of the SFG resonant amplitude A_{res} with the more intense nonresonant amplitude from the substrate A_{nr} (with $A_{nr} \gg A_{res}$) of opposite phase, the resulting SFG intensity $(A_{nr} - A_{res})^2 \approx A_{nr}^2 - 2A_{nr}A_{res}$ is composed of a wavelength-independent background A_{nr}^2 = constant and spectroscopic features $-2A_{nr}A_{res}$, which are proportional to the resonant SFG amplitude (and not to its intensity!). The peak heights of C18 resonances in solution are similar to spectra taken in air if we normalize to the substrate signal. The three peaks pertain to the methyl group and are well-known from SFG studies of long chain alkanethiolates[11,33,44−46] in air (Table 1). Two peaks correspond to the symmetric C−H stretching mode that is split into two components (r_1^+ and r_2^+ at 2878 and 2942 cm^{-1}, respectively) by Fermi resonance (FR) with the overtone of a C−H bending mode. The third peak (r^-) comprises two antisymmetric C−H stretches (2960 cm^{-1}). The Fermi resonance of the symmetric stretch at lower energy has the highest amplitude (Table 2). In accordance with earlier studies, no strong methylene resonances are found. However, a small positive peak at 2850 cm^{-1} and a negative dip at 2900 cm^{-1} might be due to the symmetric methylene stretching mode and a Fermi resonance of this mode, respectively. Infrared spectra of alkanethiolates are dominated by the symmetric and antisymmetric methylene stretching resonances at 2850 and 2920 cm^{-1},

(43) LeRille, A.; Tadjeddine, A.; Zhen, W. Q.; Peremans, A. *Chem. Phys. Lett.* **1997**, *271*, 95.

(44) Harris, A. L.; Chidsey, C. E. D.; Levinos, N. J.; Loiacono, D. N. *Chem. Phys. Lett.* **1987**, *141*, 350.

(45) Ong, T. H.; Davies, P. B.; Bain, C. D. *Langmuir* **1993**, *9*, 1836.

(46) Lampert, A. Ph.D. Thesis, University of Heidelberg (Germany), 1997.

Table 1. Vibrational Frequencies of Alkanethiols in the C−H Stretching Region: Data from the Literature and Results from This Work at the Given Electrochemical Potential[a]

	$\nu(CH_2)$, d^+	$\nu_s(CH_2)$, d_b^+	$\nu_s(CH_3)$, r^+	$\nu_s(CH_2)$, d_{FR}^+	$\nu_a(CH_2)$, d^-	$\nu_a(CH_2)$, d_{FR}^-	$\nu_s(CH_3)$, r_{FR}^+	$\nu_a(CH_3)$, r_b^- (op)	$\nu_a(CH_3)$, r_a^- (ip)
IR C_{12} acid[b]	2848	2854	2872	2901 ??	2917		2938	2954	2963
Raman C_{12} acid[b]	2845	2852	2871		2880 ??	2925	2939	2954	2965
SFG C_{16}[c]	(2852)	(2862)	2878		(2918)		2939	2954	2966
SFG Cu/C_{18} (400 mV)[d]			2874				2933		2968
SFG C_6 (350 mV)[d]			2875				2931		2968
SFG Cu/C_6 (600 mV)[d]			2871				2932		2965

[a] The peak positions are given in wavenumbers. [b] From Hill, I. R.; Levin, I. W. *J. Chem. Phys.* **1979**, *70*, 842. [c] From ref 33. [d] This work.

Table 2. Evaluation of the SFG Resonances for Cu Deposition on C18/Au(111)[a]

	r_1^+			r_2^+ (FR)			r^-			
potential (mV)	pos (cm^{-1})	width (cm^{-1})	rel ampl	pos (cm^{-1})	width (cm^{-1})	rel ampl	pos (cm^{-1})	width (cm^{-1})	rel ampl	$A^2(r^+)/A^2(r^-)$
400	2874	14	32 ± 3	2933	13	22 ± 3	2968	16	24 ± 3	5 ± 2
20	2875	17	21 ± 2	2937	15	10 ± 2	2969	23	14 ± 2	5 ± 2
−150	2878	14	31 ± 2	2938	13	15 ± 2	2967	19	21 ± 2	5 ± 1

[a] The peak relative amplitude and its experimental error are given in percent of the gold substrate signal, and peak position and the peak widths (FWHM) are given in wavenumbers.

respectively.[31,32,47−50] We remark that due to the strong dispersion of the antisymmetric mode within the alkyl chain, the corresponding Raman frequencies are 2850 and 2880 cm^{-1}, respectively.[51−53]

3.1.2. C6 Thiolate SAM. The in situ spectrum of a C6 SAM at a potential of 400 mV (Figure 5, top) exhibits the same methyl resonances as a C18 SAM. The peak intensities (Table 3) are typically a factor of 2 smaller than those for a C18 SAM, which can indicate a reduced orientational order of the C6 SAM methyl groups or a reduction of coverage to 50% with respect to C18 SAM (i.e., 16% with respect to the Au surface) in accordance with infrared and STM results for C4 SAMs.[54,55] We also find that the distribution of intensities between the lines split by Fermi resonances is different. The intensity ratio $R_{FR} = (A_1/A_2)^2$ (where A_1 and A_2 are the amplitudes of the modes r_1^+ and r_2^+, respectively) ranges from 1 (for C6 SAM, Table 3) to 4 (for C18 SAM, Table 2). Such change of R_{FR} can occur if the chemical environment of the chemical group is different, which, however, we do not attempt to interpret here. The in situ spectrum of C6 SAM on gold does not change on a time scale of 4−8 h demonstrating the stability of the system. This is due to the protecting effect of the electrolyte. In fact, it is known that the thiolate stability in air decreases with chain length.[56] Indeed, under ambient conditions we find that the amplitudes of the methyl stretching lines of C6 SAM decrease and completely disappear after about 2 h. This observation had also been previously reported by another group who exclude that only beam power or oxygen be the origin of the degradation while the exact mechanism could not yet be identified.[57]

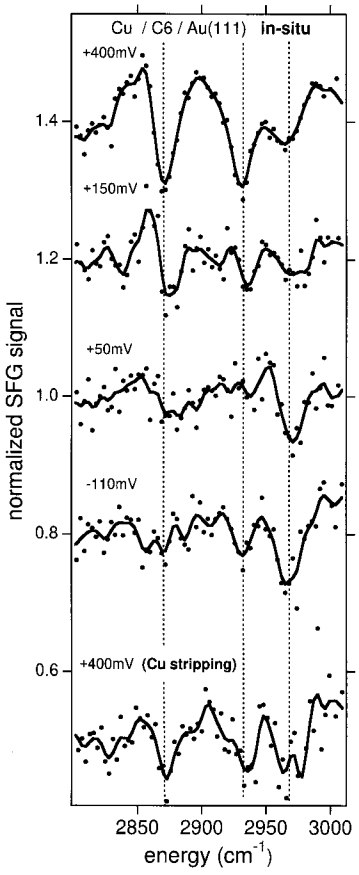

Figure 5. SFG spectra of C6 thiolate SAM/Au(111) in situ in a copper solution at different electrochemical potentials. For the presentation see Figure 4. The series exhibits a change from type I spectrum (>100 mV) to type II (<100 mV)—see also text. The measurement at 400 mV shown at the bottom is obtained after stripping off a copper film of several monolayers that had been electrodeposited before.

For the C6 SAM spectra recorded as a function of electrochemical potential (Figure 5), we distinguish three regions of electrochemical potential: The first, >200 mV where no copper can be deposited; the second, between 200 mV and 0 mV, the underpotential deposition (UPD) region where less than 20% of a monolayer of copper can be grown on Cn > 6; the third, <0 mV, overpotential deposition (OPD) conditions, where copper is continuously

(47) Stole, S. M.; Porter, M. D. *Langmuir* **1990**, *6*, 119.
(48) Badia, A.; Cuccia, L.; Demers, L.; Morin, F.; Lennox, R. B. *J. Am. Chem. Soc.* **1997**, *119*, 2682.
(49) Bensebaa, F.; Ellis, T. H. *Langmuir* **1998**, *14*, 2361.
(50) Jennings, G. K.; Laibinis, P. E. *J. Am. Chem. Soc.* **1997**, *119*, 5208.
(51) Wong, P. T. T.; Chagwedera, T. E.; Mantsch, H. H. *J. Chem. Phys.* **1987**, *87*, 4487.
(52) Rabe, J. P.; Swalen, J.D.; Rabolt, J. F. *J. Chem. Phys.* **1987**, *83*, 1601.
(53) Snyder, R. G.; Hsu, S. L.; Krimm, S. *Spectrochim. Acta* **1978**, *34A*, 395.
(54) Truong, K. D.; Rowntree, P. A. *J. Phys. Chem.* **1996**, *100*, 19917.
(55) Truong, K. D.; Rowntree, P. A. *Prog. Surf. Sci.* **1995**, *50*, 207.
(56) Schoenfisch, M. H.; Pemberton, J. E. *J. Am. Chem. Soc.* **1998**, *120*, 4502.
(57) Buck, M. Private communication.

Table 3. Evaluation of the SFG Resonances for Cu Deposition on C6/Au(111)[a]

	r_1^+			r_2^+ (FR)			r^-			
potential (mV)	pos (cm^{-1})	width (cm^{-1})	rel ampl	pos (cm^{-1})	width (cm^{-1})	rel ampl	pos (cm^{-1})	width (cm^{-1})	rel ampl	$A^2(r^+)/A^2(r^-)$
400	2871	17	16 ± 1	2932	18	17 ± 1	2965	23	10 ± 1	11 ± 2
150	2878	16	10 ± 2	2938	15	7 ± 2	2972	26	6 ± 2	8 ± 6
50	2884	31	5 ± 2			2 ± 2	2972	17	9 ± 2	0.6 ± 0.6
−110	2863	23	4 ± 2	2932	13	6 ± 2	2969	17	11 ± 2	0.8 ± 0.6
+400	2874	12	13 ± 2	2937	17	10 ± 2	2971	22	12 ± 2	4 ± 2

[a] The presentation is equivalent to that given in Table 2.

deposited, albeit with a small rate (<2 layers/h) in the presence of thiolate.

Figure 5 shows that when the potential is decreased, the spectral features of C6 SAM exhibit a discontinuous change between +50 and +150 mV. At positive potentials where no copper is deposited, the FR-split symmetric stretching vibration exhibits the largest peak height. Such spectra in which the symmetric stretching vibration at ca. 2875 cm^{-1} is the strongest (example, Figure 5, +400 mV), we will term "type I" spectra. At low potentials we observe spectra in which the antisymmetric stretch at ca. 2970 cm^{-1} is strongest (example, Figure 5, −110 mV); these we will call "type II" spectra. During Cu deposition a substantial change of the SAM structure occurs. Note that already in the UPD region the spectra change from type I to type II. Stripping off copper by returning to +400 mV (Figure 5 bottom) almost restores the original type I spectrum; however, the peaks now appear to have equal strengths, and the overall amplitudes are lower. Note that a type II spectrum with a weakened symmetric stretching mode *cannot be explained by the thiolate/Cu(111) adsorption geometry* where the alkyl chains arrange nearly perpendicularly to the surface.[3,58]

To verify that indeed copper is responsible for the spectral change, we repeated the experiments in copper-free sulfuric acid (Figure 6). Apart from a small overall loss of peak height, the spectra do not change for potentials over the whole range between 340 mV and −160 mV. However, even traces of copper in the electrolyte restore the spectral changes shown in Figure 5! The fact that small amounts, hence small coverages of copper, can lead to changes on large, if not all parts of the surface, is a remarkable phenomenon.

The results of the evaluation of the measurements for C6 and C18 are listed in Tables2−4. The peak heights are given in percent of the gold substrate signal together with the experimental error. To allow a comparison with the calculation in section 4 which does not include the FR induced peak splitting, we have to determine the SFG intensity in the absence of the FR. In infrared spectroscopy, one would have to add the intensities of both peaks. We assume that both infrared and Raman intensities scale with the square of the vibrational stretching amplitude modified due to the mixing of the FR and that the overtone possesses negligible spectral intensity. As the SFG signal can be written as a product of infrared and Raman intensities, we can then estimate the SFG intensity of the hypothetical uncoupled symmetric mode as

$$r_{tot}^{+} = (A_1 + A_2)^2 \qquad (1)$$

where A_1 and A_2 are the observed SFG amplitudes of the split line. This intensity r_{tot}^+ is given in Tables 2−4. To illustrate the shift of intensity from the symmetric to the antisymmetric mode as a function of potential, we

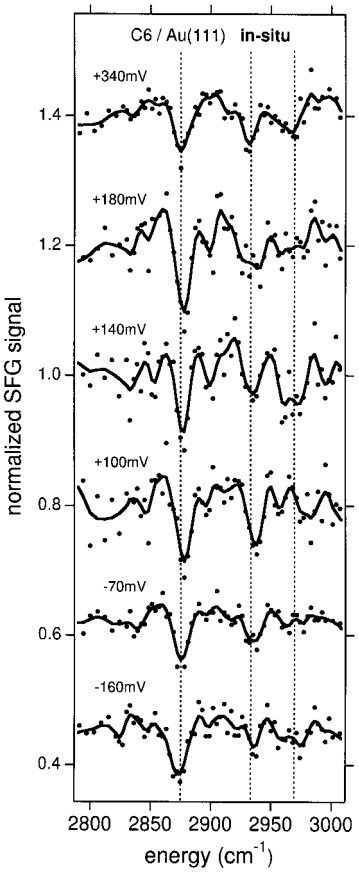

Figure 6. SFG spectra of a C6 thiolate SAM/Au(111) in situ in a copper-free solution at different potentials. For the presentation see Figure 4.

calculated (Tables 3 and 4) and plotted (Figure 7) the experimental intensity ratio r_{tot}^+/r^- for C6. Figure 7 shows that at positive potentials or in the absence of copper this ratio is around 10, while at potentials below 100 mV in the presence of copper it drops to 1. The filled triangle in Figure 7 represents the ratio after copper stripping.

3.1.3. Longer Chain Alkanethiolate SAMs. In the case of the C12 thiolate SAM (intermediate chain length) in contact with copper sulfate electrolyte, a change from type I to type II spectra occurs, but the difference is much less pronounced (Figure 8). The symmetric stretching peak loses only about half of its peak height, but the antisymmetric peak (at least in the UPD range) gains. Under OPD conditions all peaks exhibit equal height.

C18 SAM (long chain length) spectra remain type I spectra in the presence of copper and independent of electrochemical potential (Figure 4 and Table 2). In the absence of copper, very similar spectra are found in acidic electrolyte,[11] again independent of the potential.

3.2. STM Results and Discussion. The structure of electrodeposited copper on alkanethiolates is well-known for a variety of chain lengths, *n*, temperatures, and

(58) Imanishi, A.; Isawa, K.; Matsui, F.; Tsuduki, T.; Yokoyama, T.; Kondoh, H.; Kitajima, Y.; Ohta, T. *Surf. Sci.* **1998**, *407*, 282.

Table 4. Evaluation of the SFG Resonances for C6/Au(111) in a Cu-Free Solution (See Text)[a]

	r_1^+			r_2^+ (FR)			r^-			
potential (mV)	pos (cm^{-1})	width (cm^{-1})	rel ampl	pos (cm^{-1})	width (cm^{-1})	rel ampl	pos (cm^{-1})	width (cm^{-1})	rel ampl	$A^2(r^+)/A^2(r^-)$
350	2875	11	10 ± 1	2931	12	7 ± 1	2968	23	5 ± 1	12 ± 5
180	2878	12	18 ± 2	2935	24	8 ± 2	2969	26	6 ± 2	19 ± 13
120	2878	10	15 ± 3	2935	15	7 ± 3	2968	17	9 ± 3	6 ± 5
60	2878	12	14 ± 2	2938	13	11 ± 2	2983	17	6 ± 2	17 ± 12
0	2875	12	9 ± 1	2935	16	6 ± 1	2970	22	3 ± 1	25 ± 17
−160	2874	15	9 ± 1	2932	18	6 ± 1	2968	22	5 ± 1	9 ± 4

[a] The presentation is equivalent to that given in Table 2.

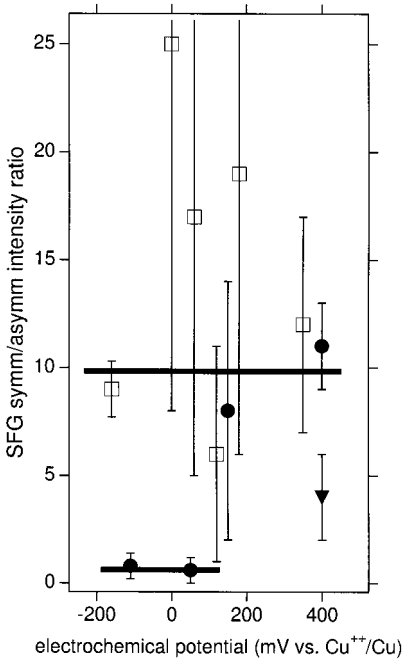

Figure 7. C6 thiolate SAM/Au(111): Ratio of the SFG intensities of the symmetric stretching mode and of the antisymmetric stretching modes (Table 2) as a function of potential. The full symbols represent the experiment with a copper-containing electrolyte. The triangle represents the stripped copper layer. The open squares are the results of the experiment with the copper-free electrolyte.

potentials.[14−16,39,59−61] In our experiments the temperature was held at 300 K and the potential was varied for n = 6, 12, and 18 in the presence of Cu (the experiments without Cu shall be discussed below). We start at a potential of 400 mV, where copper deposits neither on bare nor on thiolated gold, and then lower the potential. The most important observation is the formation of monolayer high[62] adatom islands with an average diameter of 2 nm. After completion of their formation (after ca. 2 h), the islands cover 10−15% of the surface. The islands are randomly distributed and are also found in substrate vacancies; they are not pinned to steps. Angle-resolved X-ray photoemission spectroscopy (XPS) confirmed the presence of copper on the emersed and water-rinsed surface,[16] thus we can safely assume that the islands consist of copper. We observed that the islands only form behind a "growth front" (Figure 9) in an area where the thiolate layer is imaged topographically higher than usual, corresponding to lower resistance.[63] Such areas, attaining

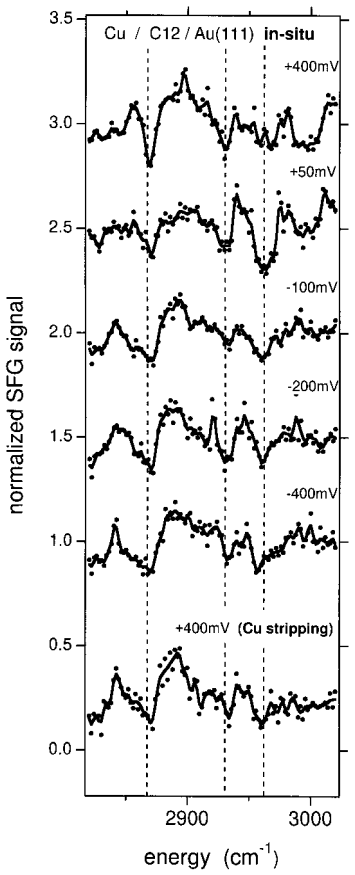

Figure 8. SFG spectra of C12 thiolate SAM/Au(111) in situ in copper solution at different electrochemical potentials. For the presentation see the caption of Figure 4.

>0.1 μm^2 after 1 h, form randomly on the sample and are not tip induced, as proven by the simultaneous observation of several areas in one image.[59] Outside the areas the normal thiolate structure prevails as exemplified by the insert at the lower right of Figure 9. Note that in this image the C6 SAM exhibits the typical stripe pattern.[54,55,64] We estimated the following coverages: copper 10%; copper-free surface 80%; island rims 10% (assuming steps with a width of two atoms, one Cu one Au).

For n = 18 this scenario is valid for *all* potentials below ca. 150 mV. For n = 6 and 12, below ca. −100 mV a pseudo-layer-by-layer growth was found: Islands grow until they coalesce; a second layer nucleates before the first is completed. Only islands already nucleated above 0 mV grow, further islands form only on existing copper islands. For n = 6 we observed a fractal shape of the growing and coalescing islands and a growth of ca. one layer per hour.

(59) Cavalleri, O. Ph.D. Thesis, EPFL, Lausanne (Switzerland), 1997.
(60) Sondag-Huethorst, J. A. M.; Fokkink, L. G. J. *Langmuir* **1995**, *11*, 4823.
(61) Hagenström, H.; Schneeweiss, M. A.; Kolb, D. M. *Langmuir* **1999,** *15*, 7802.
(62) The monolayer heights of Au(111) (0.236 nm) and Cu(111) (0.208 nm) are too similar to be distinguished in the experiment.
(63) This is in agreement with STM results by Hagenström, H.; Schneeweiss, M. A.; Kolb, D. M. *Langmuir* **1999**, *15*, 2435.
(64) Poirier, G. E. *Langmuir* **1999**, *15*, 1167.

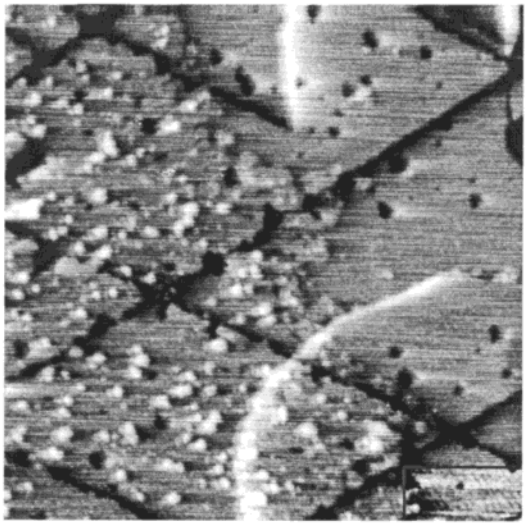

Figure 9. 228 nm × 228 nm in situ STM image showing the 2D copper island formation on a C6 SAM thiolate-covered Au(111) surface in the UPD range. Electrolyte: 50 mM H_2SO_4 + 1 mM $CuSO_4$. Electrode potential: 150 mV vs Cu/Cu^{2+}, applied for 41 min (here, the reference electrode was a copper wire). An irregularly formed border divides the right and the left part of the image. The difference in height between these two regions is much lower than that of the straight or slightly curved substrate steps. Behind this "front", on the left part of the image, copper islands (bright spots, diameters ca. 2 nm) have formed, and molecular resolution is difficult. The unaffected area (right part) exhibits the striped structure typical of a C6 SAM thiolate (see contrast enhancement on the lower right). The "front" was observed to propagate with time from the left to the right thus increasing the area covered with islands.

The coverages are now time-dependent. They change in the following way: copper 10 → 80%; copper-free surface 80 → 0%; island rims 10 → 20%.

To evaluate the influence of an electrochemical potential on an adsorbate, one has to repeat the study in the *absence* of the deposited substance. Hence we undertook an in situ STM investigation of the $CH_3(CH_2)_{n-1}S/Au(111)$ surface for $n = 6$, 12, and 18 under potential control in diluted, *copper-free* H_2SO_4. The well-known thiolate layer topography was reproduced: the surface consists of terraces, monatomic (gold) steps, and substrate vacancies that are typical for thiolate-covered gold (Figure 10a). In some cases we detected cluster-like defects that were, however, always pinned to steps (Figure 10b). This observation is valid for $n = 6$, 12, and 18 down to −200 mV, i.e., for all potential regions investigated by SFG spectroscopy. We note that Hagenström and co-workers[65] found "fronts" (which we only observed in the presence of copper) and a large number of small (ca. 4 nm diameter) gold islands under similar conditions. The reason for the difference in the results is as yet unclear. When we lowered the potential further (down to −400 mV (Figure 10c), which corresponds to very fast copper bulk deposition in 1 mM Cu^{2+} and even to hydrogen evolution), monatomic high islands with a diameter in the 5−10 nm range form ($n =$ 6, 12, and 18). Note that this diameter is clearly larger than the average copper island diameter of 2 nm.[14−16,39] For $n = 18$ and currents above 5 nA (where the tip is presumably in contact with a large number of alkyl chains), we found that steps could move by 20 nm/min.

These two observations lead us to postulate a *potential-induced gold island formation*. Generally speaking, gold

(65) See ref 63 in absence of copper; results in the presence of copper for this system (C2 SAM) are reported in ref 61.

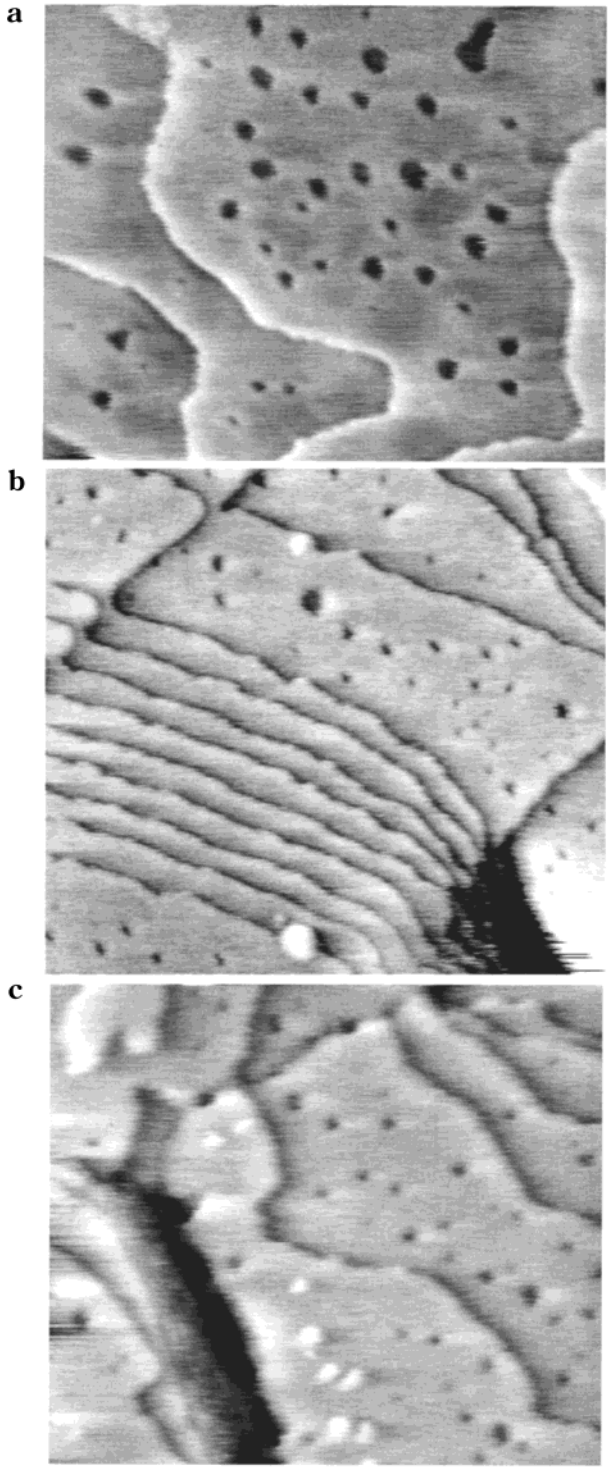

Figure 10. In situ STM images showing a thiolate-covered Au(111) surface in 50 mM H_2SO_4. The effect of different sample potentials is shown. (a) C6 SAM thiolate at −50 mV vs a hypothetical Cu/Cu^{2+} (1 mM) reference, imaged area 142 nm × 116 nm. Tunneling parameters: $I = 10$ nA, $V = 380$ mV vs sample. The white lines are substrate steps; the gray terraces show the usual substrate vacancies (black spots) that are rather large, as is typical for short chain thiolates. (b) C_{12} thiolate at −250 mV. $I = 2$ nA, $V = 300$ mV, 142 nm × 129 nm. The large black line in the lower right stems from a multistep. The potential is not yet sufficiently negative to create islands (only two bright spots attached to substrate steps are observed, but no new islands are formed). C18 exhibits the same topography. (c) Example for island formation at extremely negative potential: C18 SAM thiolate at −400 mV. $I = 25$ nA, $V = 1200$ mV, 142 nm × 125 nm. Under such conditions, islands (presumably gold, bright spots) are also found for the shorter chain lengths.

islands can form, but only at very negative potentials. Such reconstruction phenomena of adsorbate-covered metals are well-known for systems such as short-chain thiolates.[66] In these cases and also for longer chain alkanethiolates, the influence of the STM tip, especially at high tunneling currents (i.e., low distances) can become considerable. More important for us is the fact that the initial structure (at 400 mV) does not change at potentials >-200 mV. In view of the limited vertical resolution, we cannot exclude the formation of disordered structures (lower tunneling resistance corresponding to higher topography, however, with a height difference less than a substrate step), but we can exclude the formation of gold islands. The results obtained with copper are discussed in refs 14−16 and 39 and in section 1.

4. Analysis of the Orientation of the Methyl Group ($C-CH_3$ Axis)

The tilt of a molecular axis α is connected with the tilt θ of the $C-CH_3$ axis ($\alpha - \theta = 35°$, see Figure 1); hence by measuring θ, we can calculate a restricted range of possible angles α when we can exclude chain defects. In the following let us focus on the measured quantity, θ. It may appear quite evident that a reduction of the symmetric mode and an increase of the antisymmetric mode, as observed for C6 spectra with Cu adsorption (Figure 5), can be attributed to an increasing tilting of the methyl group with the $C-CH_3$ axis oriented nearly parallel to the surface. However, we want to analyze the geometry of the alkyl chain in greater detail. In infrared[67] and in Raman spectroscopy[68] the orientation of dynamic dipoles or polarizabilities on surfaces can be readily determined by comparison of spectra with different beam polarizations. Similar arguments apply to SFG spectra when additional assumptions concerning Raman tensor elements are made[69] or when large enough data sets exist.[70,71] On metal substrates p-polarized incident beams provide by far the strongest adsorbate signal. Obtaining only weak signal from the C−H stretching vibrations of the C6 SAM (<15% of the substrate signal), we have to restrict ourselves to the analysis of only this polarization combination. Its analysis requires information on the relation between χ-(2) tensor elements for symmetric and antisymmetric modes. In the ideal case, one could obtain a complete $\chi(2)$ tensor from quantum-chemical calculations.[72] However, complete calculations of the SFG tensors of the C−H stretching modes of alkanes are not available; Raman tensor elements have been calculated only for the symmetric C−H stretching modes.[73]

We thus construct the $\chi(2)$ tensors for the symmetric and antisymmetric vibrations by determining a $\chi(2)$ tensor for a single vibrating C−H bond. When we weight these tensors for different bonds with the bond vibrational amplitude in the corresponding normal vibration, we obtain an approximation of the $\chi(2)$ tensors for all modes. From this we can calculate SFG intensities in the usual way[74] accounting for the beam geometries and refractive indices of the media at the employed frequencies. The linear superposition of bond hyperpolarizabilities is, however, only a coarse approximation, see, e.g., ref 75.

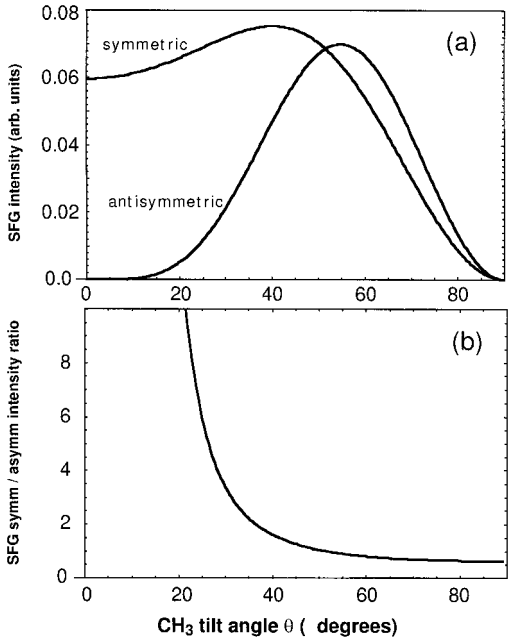

Figure 11. (a) Calculated SFG intensities in aqueous solution for the beam geometry described in the text and p polarized beams as a function of methyl group tilt θ (see Figure 1) for the symmetric and the sum of the antisymmetric stretching vibrations. (b) Intensity ratio: symmetric divided by the sum of the antisymmetric modes.

The calculated SFG intensities for the symmetric mode and the sum of the two antisymmetric modes for the parameter $\delta = 0$ (see Appendix) are plotted in Figure 11 as a function of tilt angle θ of the $C-CH_3$ axis. A sketch of the calculation is given in the Appendix. We find that a $C-CH_3$ axis oriented approximately perpendicular to the surface exhibits only intensity for the symmetric mode while the antisymmetric is not observable. A group oriented horizontally exhibits no symmetric mode (due to the horizontal infrared dynamic dipole) while the antisymmetric modes vanish due to destructive interference of signals generated by groups with different twist angle τ (Figure 1).

To test the result and specifically the choice of δ, we take the C18 SAM/Au(111) measurement at 400 mV (Figure 4 top) as a reference for which the tilt angle θ is known from literature for the ex situ case. Adding the two symmetric stretching lines from the "relative amplitude" column in Table 2, $A_1 = 32$ and $A_2 = 22$ (in arbitrary units) according to eq 1, we obtain $I_{sym}/I_{asym} = 2916/576 \approx 5$. The errors are given in Table 2. The evaluation of C18 SAM ex situ spectra[76] and in situ spectra at other potentials (Table 2) gives very similar results. Figure 11 correlates the obtained intensity ratio 5 with a tilt angle θ of about 26°. This value agrees well with the tilt angle 26.4° ± 1.8° found with a different method for C22 SAMs on Au(111) in air[46] (see also refs 23 and 25). Geometries of alkanethiol SAMs in air and in aqueous solution are similar, which

(66) This is ideally observed for the very short C2 SAM, see, e.g., ref 63.
(67) Nuzzo, R. G.; Dubois, L. H.; Allara, D. L. *J. Am. Chem. Soc.* **1990**, *112*, 558.
(68) Hines, M. A.; Harris, T. D.; Harris, A. L.; Chabal, Y. J. *J. Electron Spectrosc. Relat. Phenom.* **1993**, *64/65*, 183.
(69) Wolfrum, K.; Löbau, J.; Lauberau, A. *Appl. Phys. A* **1994**, *59*, 605.
(70) Pflumio, V.; Vallet, J. C.; Boeglin, A. J.; Villaeys, A. A.; Lavoine, J. P. *Phys. Rev. A* **1995**, *51*, 3174.
(71) Guyot-Sionnest, P.; Hunt; J. H.; Shen, Y. R. *Phys. Rev. Lett.* **1987**, *59*, 1597.
(72) Pouthier, V.; Ramseyer, C.; Girardet, C. *J. Chem. Phys.* **1998**, *108*, 6502.
(73) Gough, K. M. *J. Chem. Phys.* **1989**, *91*, 2424.
(74) See, e.g., *The Principles of Nonlinear Optics*; Shen, Y., Ed.; John Wiley & Sons: New York, 1984; Akamatsu, N.; Domen, K.; Hirose, C. *J. Phys. Chem.* **1993**, *97*, 10070.
(75) Gussoni, M. In *Advances in Infrared and Raman Spectroscopy*; Clark, R. J. H., Hester, R. E., Eds.; Heyden & Son: Philadelphia, 1980; Vol. 6.
(76) Epple, M. Ph.D. Thesis, EPFL, Lausanne (Switzerland), 1999.

is reflected in SFG spectra that do not differ for these two cases. The precision of agreement between calculation and literature value might in part be fortuitious but indicates that the calculation represents a reasonable estimate.

Applying the same evaluation to the C6 SAM, we find in the range where no copper is deposited (400 and 150 mV) $I_{sym}/I_{asym} \approx 10$ (Table 3), which indicates an insignificantly smaller tilt ($\theta = 22°$) than that seen in the case of the C18 SAM. For copper deposition (potentials 50 and −110 mV) where the intensity of the symmetric stretching mode has almost disappeared, the ratio is still around 0.7 (Table 3). This means that contrary to a superficial inspection, the symmetric mode has still about the same SFG intensity as the antisymmetric mode. It is, in fact, in agreement with the result of the calculation (Figure 11) in the range $60° < \theta < 90°$ and demonstrates that eq 1 holds in our case. Calculations carried out in the range $0.25 > \delta > 0$ also yield results for which the intensity sum of the antisymmetric modes is never stronger than the intensity of the symmetric mode. The intensity ratio is no more sensitive to the tilt angle θ above 50° (Figure 11 bottom). We thus have to analyze also the changes in peak height. Between +150 and +50 mV the symmetric mode is reduced by a factor of 3 while the sum of the antisymmetric modes stays about the same (Table 3). We obtain a tilt angle θ at potentials <50 mV of 83 ± 1.5°. The error of the result is obtained by error propagation from the experimental result via the curve in Figure 11, which we assume as a valid estimate. As the angle between the $C-CH_3-$ group axis and chain is 35° (Figure 1), the tilt angle of the chain α must in any case be larger than 48°. This excludes a geometry in which the thiolate backbone is perpendicular to the surface plane.

By stripping the deposited copper off the gold surface, the intensity ratio moves back to a value of about 4 (Table 3), which corresponds to a tilt angle θ of 30 ± 7°, similar to the original value before copper deposition. *Hence the tilt change is reversible with respect to copper deposition.*

We summarize the results of modeling the SFG intensity from the methyl group in saying that for the C6 SAM the $C-CH_3$ tilt angle θ changes from about 22° to 83° when copper is deposited at potentials lower or equal to +50 mV.

5. Discussion

5.1. Orientational Change of the Methyl Group in the C6 SAM. We will now discuss possible structures of the thiolate that may correspond to the observed spectra. As the C6 SAM may, in fact, be composed of domains of different structures, we have to restrict ourselves—as in the quantitative analysis above—to a discussion of a single "average" structure which corresponds to the majority of adsorbates on the surface and is the only structure that determines the intensities in the spectra.

We can safely assume that the C18 SAM will be better ordered than the C6 SAM due to the longer chain length which stabilizes ordered structures in C18 SAM. As in our experiment the peak height in the symmetric stretch mode is proportional to the coverage by the upright molecular species, we can evaluate the ratio in peak height of the symmetric mode between C18 and C6 SAM. For the C6 SAM (at 400 mV) we can still observe a density larger than 50% of the C18 SAM density (i.e., a coverage of 16%). Even after copper stripping we can still account for a density larger than 30% of the C18 SAM. These values can be taken as lower limits of the total thiolate coverage.

Our STM results show that the island rims represent only some 10% of the surface (see section 3.2) which excludes that the spectra are dominated by (probably tilted) thiolate at step edges. We can also exclude that defects generated locally (e.g., during the adsorption of single copper atoms) can lead to the changed spectra.

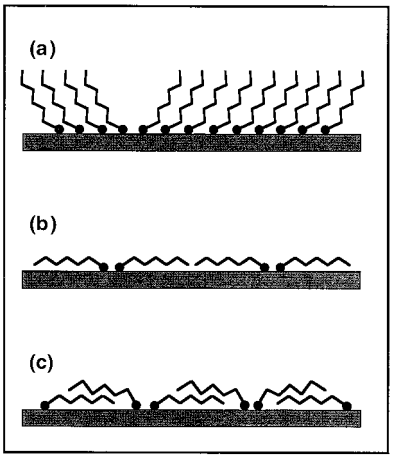

Figure 12. Illustration of possible structures of the short-chain thiolates on Au(111). (a) Close-packed $\sqrt{3} \times \sqrt{3}$ structure with chains tilted by $\alpha \approx 30°$ with respect to the surface normal. On the left-hand side a domain boundary is drawn. (b) Striped phase with alkane chains parallel to the substrate. (c) Striped phase with "interdigitation". This phase possesses a high density of gauche defects.

In the SFG spectra methylene stretching peaks are at least 1 order of magnitude smaller than methyl peaks. A calculation following the lines of the calculation in section 4 but extended to methylene groups allows us to estimate roughly that there is less than one conformational defect (cis or gauche defect) per six observed methyl groups. Thus defects in the backbone are unlikely to play the key role in the copper-induced tilting of the methyl group. However, certain types of conformation can remain unobserved. First, cis conformations cannot be observed by SFG for chains with molecular twists near $\beta = 90°$ (see Figure 1). In this geometry the defect conserves the angle of the backbone (and of the methyl group) with respect to the surface plane. Second, a g^+ t g^- sequence in which two gauche defects with opposite rotation directions are separated by a trans conformation conserve the local inversion symmetry in the chain[77] and would not appear in the SFG spectrum. Possible structures for the C6 phase in the presence of copper are thus: a *flat phase* or an "*interdigitation*" *phase*[64] (see Figure 12) which may contain the two described types of defects.

The type II spectrum is not typical for the structure of thiolate SAMs on copper.[3] With copper as a substrate, the thiolate backbone is expected to rather "stand up" and form a phase similar as on Ag although not as well ordered.[78] However, our result indicates that the backbone is tilted by $\alpha > 48°$ (section 4). The type II spectrum also does not represent a phase containing disordered alkyl chains that would be indicated by weakened methyl resonances and by the appearance of methylene peaks.

As the experimental results clearly exclude a changed structure only due to the electrochemical potential, the change must be due to the presence of Cu at low potentials. The still low substrate defect density after copper deposition found by STM and the fact that a type II spectrum

(77) Goates, S. R.; Schofield, D. A.; Bain, C. D. *Langmuir* **1999**, *15*, 1400.

(78) The preparation of copper surfaces is very difficult without vacuum techniques due to their extremely oxophilic nature (Hartinger, S.; Doblhofer, K. *J. Electroanal. Chem.* **1995**, *380*, 185.), often resulting in poor reproducibility, also of adsorbed thiolate SAMs, see ref 31.

cannot be explained by typical adsorption geometries of thiolates on copper suggest that the chemical and morphological changes at the substrate are not essential. On the other hand, copper must penetrate the thiolate since it is found below the organic layer after deposition.[16] It is thus likely that the penetrating copper affects the alkyl chains directly.

Structural changes in thiolate SAMs were often found to be reversible, e.g., when they are induced by high temperature[15,26,49] or by a change of solvent[28,45] ("weak activation" according to Cavalleri et al.[16]). Similarly, one might assume a continuous increase of defect density due to increasing Cu coverage or due to increasing penetration into the thiolate layer during deposition. On the other hand, the thiolate layer apparently "switches" between different geometries once the copper starts to adsorb: No continuous change between type I to type II spectra was found as a function either of potential or of deposition time. A possible scenario is that when the potential decreases, the (solvated) Cu ion or atom concentration in the thiolate layer increases, i.e., *copper penetrates the organic layer, and triggers at a certain concentration a transition to a different structure*. For this process we cannot determine at which stage the electrons are transferred, i.e., when the ion is reduced (the formation of the Au−Cu interface determines the energetics of the deposition while the kinetics is controlled by the penetration[16]). Although the identification of the detailed mechanism and the driving force for the transition require further investigation, one may speculate that similar transitions can occur for other surfactant systems.

We propose a simple path to transform structure I into structure II *without* a substantial increase of the chain tilt α: a "rolling" motion, i.e., a rotation by angle β (see Figure 1). In this way the $C-CH_3$ axis that is initially nearly perpendicular ($\alpha = 30°$ and $\beta = 45°$ [46]) can align almost parallel to the surface ($\alpha = 48°$ and $\beta = 180°$). The tilt now increases by only 18°. Such a small change might indeed be triggered by local defects such as penetrating copper while large changes necessitate "strong activation" such as desorption.[16] It is important to remark that the proposed rotation changes the angle ξ (surface−S−C angle, see Figure 1) from 110° to 180° and hence the sulfur hybridization from sp^3 to sp. These two types of bonding have been found to be energetically similar for thiolate systems.[19,24] The proposed geometry can thus coherently explain the observed substantial spectral change by a relatively small energetic change of the system.

5.2. Order/Disorder. Copper deposition appears to proceed in STM studies qualitatively similar for all SAMs in the range C6−C18 although the rates decrease strongly. For the same range of systems it differs, however, qualitatively in SFG spectroscopy. Again, we can evaluate the complementary information obtained by the local and the global method. Before copper islands form, a so-called "front" is detected with STM (Figure 9) for all chain lengths.[14,39] We observed that only the area behind a front was able to express copper islands. In such an area the tunneling resistance is lowered, and no ordered adsorbate structures can be resolved. The measured SFG spectra must contain substantial intensity from these areas, but they exhibit no change of peak positions and amplitudes and no additional (i.e., methylene) bands. We conclude that the structural modification which occurs behind the front and whose microscopic origin is not yet clearified does not affect the conformation of the backbone (e.g., gauche defects) or the orientation of the methyl group.

This fact, combined with the idea that STM at nanoampere current probes mainly the sulfur headgroup and is not sensitive to conformational changes of thiolates, leads us to propose *for C18 a disorder of the sulfur packing* (*observed by STM*) *while the chains essentially retain their conformation* (*observed by SFG*) (see theoretical studies[17,18]). The penetration of aluminum into SAMs[79] appears to be based on similar processes. Also SAM formation and healing processes are based upon sulfur mobility and (initial) disorder. In passing, we note that disorder within a dense SAM leads to the suggestion of other sulfur adsorption sites than the standard 3-fold hollow site Au_3.[17−19,22]

5.3. Density/Stability. Our in situ results confirm that the structures of *C6 and C18 SAM are stable and virtually unchanged in electrolyte* as already found by Hines et al.[11] for C18 SAM (SFG spectroscopy in $HClO_4$) and by Anderson et al.[12,13] for C18 and C14 SAMs (infrared spectroscopy in D_2O). The observation is understandable since water and ions interact very weakly with the only accessible moiety, the methyl group. The C18 and C6 SAM structures do not change in the absence of copper, even if electrochemical potentials are tuned over a wide range.

5.4. Surfactant Behavior. For all cases, especially when we compare copper and copper-free electrolyte, the observed SFG intensities are similar. If copper were to adsorb on top of a SAM, the resonances in the SFG spectra would change drastically for both C6 and C18. In the SFG experiments we can thus follow the surfactant behavior in situ from the adsorbate point of view. The fact that we can strip off the copper and still obtain intense resonances shows in addition that only a small part of the SAM desorbs during the stripping and even less (if any at all) during Cu deposition.

6. Conclusion

The combination of in situ SFG spectroscopy and in situ STM gives insight into the behavior of SAMs under electrochemical control with and without metal deposition. Comparison of results obtained by the two methods demonstrates that spatial disorder during Cu deposition probed by STM is not accompanied by strong conformational disordering of the layer. SFG spectroscopy proves that during copper deposition the investigated thiolates behave as surfactants.

While both C6 SAM and C18 SAM form layers which remain unchanged even over a large potential range in Cu-free aqueous solution, we observe a reversible molecular reorientation of C6 even during the deposition of submonolayer coverages of Cu. The SFG spectra show that the methyl group axis becomes oriented almost parallel to the surface, however, without indication of substantial desorption of the SAM. The Cu deposition induced structure differs from typical defect structures (e.g., formation of gauche defects) and cannot be assigned to the structure of thiolates on a Cu surface. The results are consistent with a rotation of the thiolate molecule around its axis, which is related to a change of bond hybridization at the sulfur group.

Acknowledgment. We thank O. Cavalleri for providing the Cu/C6 SAM STM image. A.M.B. thanks the Alexander von Humboldt Foundation for a Feodor Lynen Research Fellowship (EPFL, Lausanne) and the Fondation National Alfred Kastler for a grant (LURE, Orsay). M.E. and A.M.B. thank O. Pluchery for his valuable help in Orsay.

Appendix

In this appendix we give a more detailed outline of the calculation; a detailed description will be presented in a

(79) Allara, D. L.; Nuzzo, R. G. *Langmuir* **1985**, *1*, 52.

forthcoming paper.[80] To start with, we assign to the C−H stretching vibration a dynamic dipole of (relative) magnitude 1 parallel to the bond and a diagonal Raman tensor with the (relative) magnitude 1 in the *zz* component where *z* is the direction of the C−H bond. The two other diagonal elements of the Raman tensor are given the value δ. The outer product of the dipole vector and the Raman tensor gives us the C−H bond tensor $\chi(2)$. The methyl vibrational eigenmodes are obtained assuming that the mass of the C atom is large compared to H thus providing straightforwardly eigenvectors with respect to the three bond lengths u_i as $(u_1,u_2,u_3)=(1,1,1)/\sqrt{3}$ (symmetric mode) and $(-2,1,1)/\sqrt{6}$ and $(0,1,-1)/\sqrt{2}$ (degenerate antisymmetric modes). We then add the bond-$\chi(2)$ tensors, each properly oriented in space and each weighted with the bonds' vibrational amplitude and obtain the $\chi(2)$ tensor of the methyl group.

In this oversimplified calculation we introduced a single adjustable parameter δ. To determine δ we calculate the Raman tensor for the symmetric stretching mode in the $C-CH_3$ coordinate system. Assuming a value $\delta = 0$, we obtain a ratio between the *xx* and the *zz* components of 0.77/0.20 = 4.2. This gives us a Raman depolarization ratio (ratio of scattered light for differently polarized *incident* light) of $\rho_n = 0.12$ in good agreement with the values for methyl groups attached to long alkyl chains.[81] We believe that this adjustment is more adequate than fitting δ to the depolarization ratio of the symmetric methyl stretch vibration of liquid ethanol,[82] which would give $\delta = 0.25$. The effect of such an increased δ value in the final result is essentially to make the SFG signal of the antisymmetric vibration substantially weaker than the symmetric vibration.

With the properly added $C-CH_3$ group $\chi(2)$ tensors the SFG intensity is then obtained as

$$I_{SFG} = \text{constant } |\chi^{(2)}:L_{SFGp}F_{vis}F_{IR}|^2 I_{IR}I_{vis} \qquad (2)$$

We compute the Fresnel factors *F* and *L* for beams incident in water ($n(3.3\ \mu m) = 1.42$, $n(0.4-0.6\ \mu m) = 1.34$) at incidence angles $\vartheta_i^{IR} = 56°$, $\vartheta_i^{vis} = 70°$, and the SFG radiation angle $\vartheta_f^{SFG} = 69°$ (see Experimental Section) with gold crystal refractive indices $n(3.3\ \mu m) = 1.25 - 17.6i$, $n(0.53\,\mu m) = 0.46 - 2.27i$, $n(0.45\,\mu m) = 1.53 - 1.86i$ from ref 83.

If molecules in different orientations are present at the surface, averaging has to be done within the norm signs in eq 2, which is equivalent to averaging of the $\chi^{(2)}$ tensor. Because at room temperature the methyl group can freely rotate around its group axis (τ-axis, see Figure 1) averaging of $\chi(2)$ over all twist angles τ of the $C-CH_3$ axis is carried out. This corresponds to a coherent superposition of the emitted radiation. However, it has been shown that the vibrational frequency depends on the position during this rotation of the group,[84] which suggests that a partially incoherent superposition (averaging of intensities) might also be adequate.

As the adsorbate is adsorbed on a flat surface and we observed the same spectra for polycrystalline samples and crystalline samples in different orientations, we average over all azimuthal orientations ϕ of the molecules. The full calculation—including ϕ as a parameter—shows that, in fact, the SFG signal does not vary strongly with azimuthal angle.

LA0109819

(80) Kuhnke, K.; Epple, M.; Bittner, A. M.; Kern, K. In preparation.
(81) *DMS Raman/IR Atlas of Organic Compounds*; Schrader, B., Merier, W., Eds.; Verlag Chemie: Weinheim, 1974.
(82) Colles, M. J.; Griffith, J. E. *J. Chem. Phys.* **1972**, *56*, 3384.
(83) *American Institute of Physics Handbook*; Hass, G., Hadley, L., Eds.; McGraw-Hill: New York, 1972.
(84) MacPhail, R. A.; Snyder, R. G.; Strauss, H. L. *J. Chem. Phys.* **1982**, *77*, 1118.